

In-beam tests of a ring imaging Čerenkov detector with a multianode photomultiplier readout

R. Debbe, S. Gushue, B. Moskowitz, J. Norris¹, J. Olness,
F. Videbæk

Brookhaven National Laboratory, Upton, New York 11973, USA

Abstract

A ring-imaging Čerenkov counter read out by a 100-channel PMT of active area $10 \times 10 \text{ cm}^2$ was operated successfully in a test beam at the BNL AGS with several radiator gases, including the heavy fluorocarbon C_4F_{10} . Ring radii were measured for electrons, muons, pions and kaons over the particle momentum range from 2 to 12 GeV/c , and a best resolution of $\sigma_r/r = 2.3\%$ was obtained.

1 Motivation

Ring Imaging Čerenkov (RICH) counters are powerful tools for achieving particle identification over a wide range of momentum within a single detector. The experience of the SLD[1,2] and DELPHI[3,4] Collaborations in developing broad-range detectors has shown that $\pi/K/p$ separation can be achieved up to approximately 30 GeV/c and e/π separation can be performed up to 6 GeV/c . There is also the capability of handling modest multiplicities within the detector. For reviews on the subject, see Refs. [5] and [6].

For a given particle the frequency distribution of Čerenkov radiation, $dN/d\nu$, is constant for all frequencies, ν , leading to several possible photon detection schemes. Existing RICH counters generally detect the Čerenkov photons in the UV region (6.5 – 7.5 eV) by means of photoionization of a complex organic molecule, such as TMAE or TEA, in a gas chamber. Alternatively, a segmented optical readout based on an array of photomultipliers offers four main advantages over the gas-based chamber:

¹ Now at Department of Physics, Kansas State University, Manhattan, KS 66506.

- (1) No special handling for hazardous materials, such as gaseous photocathodes.
- (2) No need for the high purity UV-transparent materials called for when detecting photons of energy greater than 6 eV ($\lambda < 200$ nm), such as is the case for gaseous photocathodes as well as CsI photocathodes.
- (3) Greater overall integrated efficiency due to the wide bandwidth (2.5–4.3 eV) of the photocathodes used in PMT's.
- (4) The possibility of readout fast enough for first-level triggering of the host experiment.

For these reasons, the proposed BRAHMS Experiment[7] at RHIC plans to use such a RICH counter to perform the high momentum particle identification for a forward-angle ($2^\circ < \theta < 18^\circ$) spectrometer. This counter is designed to identify pions in the momentum range from 4 to 20 GeV/ c , kaons from 9 to 20 GeV/ c , and protons from 17 to 35 GeV/ c . To obtain the high index of refraction necessary for the required coverage ($n=1.00185$), a radiator of gaseous perfluorobutane (C_4F_{10}) at 1.25 atm. absolute pressure has been selected. For photon detection, the BRAHMS design calls for four 100-anode PMT's forming a two-by-two array, each with an active area of 10×10 cm², as described below. Although arrays of single-anode PMT's[8], as well as an image intensifier coupled to a CCD readout[9], have been used successfully in previous RICH counters, state-of-the-art large-area multi-anode PMT's offer the advantage of many channels with a single common power supply and a fast, compact readout. For more details concerning the BRAHMS RICH counter, see Refs. [7] and [10].

Key elements of the proposed RICH detector have been subjected to in-beam testing using momentum-selected secondary beams at the BNL AGS, namely:

- (1) Use of the heavy fluorocarbon C_4F_{10} gas radiator to provide a high index of refraction at near-atmospheric pressures.
- (2) Use of a large-area (10×10 cm²) segmented multi-anode PMT for fast imaging of the various ring patterns.
- (3) An off-axis displacement of the focal plane, obtained by a rotation of the focussing mirror, such that the focal plane detector is situated outside the radiator volume illuminated by the particle flux.

Some pertinent results of these tests (RHIC R. & D. Project 44) are reported here. Note that the multi-anode PMT used in these measurements was the first product of a new design by the Hamamatsu Corporation[11]. The expected performance criteria outlined in Ref. [7], based upon Hamamatsu's specifications, are largely borne out by the present results.

2 The Multi-anode PMT

The Hamamatsu R-4549-01 is a 20-stage 100-anode PMT based on a fine-mesh dynode structure, providing a current gain of 3×10^6 at a high voltage of HV = -2000 volts. In this model a special grid of focusing electrodes has been installed between the photocathode and the first dynode which is designed to improve the spatial resolution and uniformity as seen in the individual anode signals (i.e., pixel response). The 10×10 cm² photocathode is bialkali; the segmented anode is a matrix array ($10 \times 10 = 100$) of 9.5×9.5 mm² units with lemo outputs. (The outer glass envelope of the PMT measures 12.8×12.8 cm².) With current gains from 10^6 to 2×10^7 (HV = -1800 to -2500 volts) the outputs will easily drive cable connections to appropriate ADC's. The high voltage is supplied by a single high-voltage cable: a built-in R/C dropping chain fixes the relative dynode voltages. A single output from the last dynode, representing essentially the "sum" of all anode currents, is available as a convenient trigger.

The entrance window is of boro-silicate glass with the typical cutoff for wavelengths $\lambda < 300$ nm ($E > 4.1$ eV). The quantum efficiency response function is approximately Gaussian, with a peak sensitivity of 18%, centered at $E = 3.4$ eV and with FWHM = 1.8 eV. (The tails, however, fall off twice as fast as a true Gaussian.) The integral of the PMT quantum efficiency, ϵ , over the photon energy, E , is $\int \epsilon(E)dE = 0.33$ eV. The efficiency was found to be fairly uniform over the central region of the PMT face, with a fall-off of 30-50% at the edges and corners, respectively.

3 Measurements of the PMT Response

Since the Čerenkov ring-image is composed of multiple hits of single photons, we were prompted to study the single-hit response. For this purpose, the R-4549 PMT was first mounted in a light-tight box. A photon source was made by collimating the light from a blue LED. The collimator opening was positioned a few millimeters away from the photocathode, and was such as to illuminate only a single pixel at a time. The LED was pulsed by a driver whose intensity could be tuned low enough so that the collimator output was either 0 or 1 photon. (This tuning requirement was checked independently using an RCA 8854 PMT with excellent single-photon resolution.) The data acquisition was triggered by the same signal which triggered the LED. Figure 1a shows the ADC pulse height distribution for a typical pixel. This distribution is exponential in shape with no distinct separation of the pedestal from a one-photoelectron peak. By contrast, the ADC distribution for the RCA tube, shown in Fig. 1b, shows such a separation.

The position dependence of the response is shown in Fig. 2. The relative pulse height in each of three adjacent pixels is plotted for a run in which the position of the LED relative to the phototube was stepped in the y -direction. (To improve the signal, the voltage driving the LED was raised so as to produce many photoelectrons.) The FWHM of the response for an individual pixel is 10 mm with little cross-talk between neighboring pixels, as expected. The pulse heights in neighboring pixels average only about 10% of that in the hit pixel for a hit in the center.

4 The Prototype Detector

The prototype RICH counter is shown schematically in Fig. 3. It was constructed from 1.9 cm thick aluminum plate, vacuum-welded at the box edges, with a removable top attached by 50 1/4-20 screws and sealed by a rubber gasket. The inner dimensions are $127 \times 64 \times 46$ cm³. The particle beam enters via a 15 cm diameter mylar window of thickness 0.025 cm (shown on the left in the figure) and exits through an identical window at the output port.

A 15 cm diameter concave glass mirror[12] whose front surface has been aluminized with a protective MgF₂ coating and which has a focal length $f = 91.4$ cm is situated at a distance of $L = 114.3$ cm from the beam entrance. This mirror is rotated by an angle $\alpha = 8^\circ$ relative to the beam direction, producing a ring image focussed at $2\alpha = 16^\circ$. The reflectivity of the mirror is approximately 80–90% at visible wavelengths. The mirror is mounted in a frame attached to an axle which can be rotated about a vertical axis perpendicular to the beam direction. The mirror angle is controlled by a 0.6 cm steel rod which moves a 47 cm arm rigidly fixed to the mirror frame, so as to allow a mirror rotation over the range $-12^\circ < \alpha < +12^\circ$. Due to practical space constraints, the position of the front face of the phototube was at a distance of 84.5 cm from the center of the mirror, causing images on the photodetector to be very slightly out of focus. In fitting experimental ring patterns we adopted an effective focal length reduced by 3% from the true focal length to account for the displacement from the focal plane.

One hundred six Lemo signal cables are fed into the box using ordinary Lemo feed-throughs epoxyed into place to maintain a vacuum seal. The output signal from each of the PMT anodes is fed into an input channel of a LeCroy 1882 Fastbus ADC for readout of the pulse height.

The device was aligned in the secondary test beam at the AGS, with the trigger defined by a 2×2 cm² scintillator, S1, just before the entrance window of the test vessel, and a larger scintillator paddle, S2, downstream of the exit window. The initial alignment was accomplished using a laser placed on the

known beam axis; the mirror and detector angles were then set and checked visually.

Two identical drift chambers, one 57 cm in front of and one 79 cm behind the prototype counter, provided tracking for determining the particle trajectory. These two chambers are part of a set of four wire chambers built for the tracking system of BNL Experiment 878 and used during the 1991 and 1992 heavy ion runs. Each chamber consists of six planes with wires oriented in three sets of directions. For each wire orientation an offset of half a cell size provides the information necessary to resolve the left-right ambiguity present in these wire detectors. The position resolution for each plane of the drift chambers has been measured as being 150 μm . Thus, the expected position of the center of each RICH ring on the phototube is determined to a resolution of approximately 500 μm in both the x and y directions.

5 Radiator Gases and the Gas Handling System

C_4F_{10} (perfluorobutane) is a colorless, odorless, non-flamable gas which is essentially inert. In other respects, save for flamability, it resembles its hydrocarbon counterpart, butane. The most abundant form resulting from commercial production is the n-isomer, a completely fluorinated linear carbon chain. Table 1 presents a comparison of key properties for this and other radiator gases used in the results presented here. The optical transmission of a sample of the C_4F_{10} gas used in the measurements reported here was recorded with a UV spectrometer, and it was found that the transmission of this gas is nearly 100% at wavelengths of 230-450 nm. The DELPHI Collaboration reports[4] complete transparency of pure C_4F_{10} at shorter wavelengths down to 160 nm.

The gas-handling system used in filling the RICH chamber with fluorocarbons is shown in Fig. 4. The procedure adopted utilizes the fact that the radiator gases Freon-12 (122) and C_4F_{10} (238) have molecular weights (given in parentheses) much heavier than air (29) or argon (40). For example, consider the case where the RICH chamber has been initially filled with argon. The C_4F_{10} , which is supplied by PCR, Inc.[16], is set to flow slowly into the bottom of the vessel, while the output mixture ($\text{Ar} + \text{C}_4\text{F}_{10}$) is sent through a cooled recovery tank where the C_4F_{10} is liquified while the argon passes out through the exhaust. The differing (by a factor of 6) molecular weights result in a density gradient in the RICH vessel, such that if the flow is slow enough (non-turbulent) the volume slowly becomes enriched in C_4F_{10} . The procedure can be continued until the supply in tank A is exhausted. In our case we manually switched the two tanks A and B and repeated the cycle using the C_4F_{10} previously recovered in B. Three such cycles yielded a gas mix of approximately 90% purity in C_4F_{10} .

In order to recover the C_4F_{10} at the conclusion of the experiment, a pump was used to reverse the flow direction, as indicated by the dashed lines in Fig. 4. As the C_4F_{10} is recovered into B, the observed pressure drop in the chamber is compensated by adding argon to maintain a pressure differential of < 0.15 atm.

In principle, one can install a remote-controlled switching system to actuate the controlling valves, so as to alternate the designated function of the supply and recovery tanks. This would allow an extended period of automatic cycling, leading to a nearly 100% purity of C_4F_{10} , or by reversing the cycle, a complete recovery of the fluorocarbon.

6 In-Beam Test Results

Figure 5 presents results measured with the beam tuned for negative 12 GeV/ c particles — predominantly pions — and a gas mixture in the test box of Freon-12 and N_2 . The squares plotted in panel (a) are proportional in size to the pulse height for each phototube pixel, summed over approximately 1100 events. The drawn ring is the best fit of the data to a circle. Figure 5b is a histogram of the ADC pulse height in pixel (3,8), which lies directly on the ring. Note the similarity to Fig. 1a. The corresponding histogram from neighboring pixel (3,9), which is not on the ring, is shown in Fig. 5c; clearly the cross-talk between adjacent pixels is small, although not completely negligible.

The ability of the counter to identify individual particles is demonstrated in Fig. 6. Panels a, b and c show individual events from a run where the beam momentum was tuned to 3 GeV/ c and the box contained a C_4F_{10} -Ar mixture. The drawn rings show the best fits (see below) to circles constrained by the positions of the ring center (shown as the small star symbols) given independently by the drift chamber tracking. The ring radius from all events in the run is histogrammed in Fig. 6d where three distinct peaks, identified with π^- , μ^- and e^- , are clearly observed. The peaks are well described as Gaussian in shape; for the rings which are fully saturated in radius (electrons) the resolution of the radius determination is $\sigma_r/r = 2.3\%$.

The fitting procedure extracted the ring radius by means of the ADC-weighted average of the distances from pixel centers to the ring center given by the tracking. Exhaustive simulations of this ring-fitting algorithm show negligible bias for rings of radius from 2.0 to 4.2 cm, and predict a resolution of approximately half of that actually achieved. The remaining contribution to the measured resolution can be attributed to chromatic and geometric aberrations (see discussion in Ref. [7]).

7 Momentum Scan

A momentum scan was performed with a C_4F_{10} -Ar mixture in the vessel during a period in which the mixing proportion of the two gases was held fixed. The ring radius is plotted versus momentum in Fig. 7, which shows saturated light production from electrons, as well as the excitation curves for muons, pions and kaons. The saturated radius for electrons implies an index of refraction $n=1.00113$, shown as the horizontal line through the electron points. The excitation curves predicted by this index of refraction are shown as the solid curves; the shaded regions represent a $\pm 5\%$ systematic uncertainty in the absolute momentum scale. The measured values of the radius all lie within the shaded regions, giving confidence that the particle identification is correct. From $n=1.00113$ it is inferred that the fraction of C_4F_{10} in the vessel was approximately 75%. Later runs following further filling of the vessel achieved approximately 90% C_4F_{10} .

8 Photoelectron Yield and the Figure of Merit

The difficulty in determining the photoelectron yield precisely can be understood from examination of the single-pixel response functions illustrated in Fig. 5b and c. The wire-mesh dynode structure of the H-4549 PMT does not provide the typical Gaussian response function which would allow one to distinguish 1, 2 or 3 photoelectron hits. Rather, the exponential shape of the response function makes it difficult to determine for a given event the number of hits on an individual pixel.

The yield was instead deduced from the distribution of the anode ADC sum (pedestal and gain corrected) per event. For the case of the C_4F_{10} -Ar mix mentioned in the previous section and 12 GeV/c pions, the ADC sum distribution perfectly describes a gaussian curve whose mean is 699 and r.m.s. width is 185; hence the number of photoelectrons is $(699/185)^2=14.3$, and the figure of merit is approximately 60 cm^{-1} . Although this value is somewhat lower than the expected value of 90 cm^{-1} , as based on the manufacturer's specifications for the mirror and PMT, it suffices for the design criteria of BRAHMS[7].

9 Conclusions

All three key elements of the BRAHMS RICH counter, namely the use of C_4F_{10} gas, the use of the large area multi-anode PMT, and the off-axis displacement of the focal plane, were successfully tested together. Particle identification was

possible on an event-by-event basis by determining the Čerenkov ring radius to a resolution of $\sigma_r/r = 2.3\%$, which is quite close to the design value in Ref. [7]. Improvement in the systematic understanding of the ring radius versus momentum curves (see Fig. 7) is planned for future measurements which will include determination of the particle momentum by time-of-flight techniques and direct measurement of the radiator index of refraction using a Fabry-Perot interferometer.

Acknowledgements

We would like to thank E. Hergert and S. Suzuki of Hamamatsu Corp., as well as K. Arisaka of UCLA, for useful discussions and developments on the special multi-anode PMT used in this work. We also thank our colleagues, C. Chasman, H. Hamagaki and T. Sugitate, for their interest and assistance in the initiation of this investigation. Consultations with R. Du Boisson, of PCR Inc., on the nature of the fluorocarbon gases is also gratefully acknowledged. We also want to thank R.A. Holroyd of the BNL Chemistry Department for his measurement of the UV transmission of C_4F_{10} . This work was supported by U.S. Department of Energy contract number DE-AC02-76CH00016, in part through the R.&D. funds of the RHIC Project, and we thank T. Ludlam for his encouragement in this enterprise.

References

- [1] V. Ashford, et al., presented at the XXIII Int. Conf. on High Energy Physics (Berkeley, CA, July 16–23, 1986) SLAC-PUB-4046; V. Ashford, et al., IEEE Trans. Nucl. Sci. **NS-34** (1987) 499.
- [2] SLD Collaboration, Nucl. Instrum. and Meth. **A343** (1994) 74.
- [3] DELPHI Collaboration, Nucl. Instrum. and Meth. **A303** (1991) 233.
- [4] DELPHI Collaboration, Nucl. Instrum. and Meth. **A343** (1994) 68.
- [5] T. Ypsilantis, *Proc. of the Symposium on Particle Identification at High Luminosity Hadron Colliders*, T. J. Goulay and J. G. Mofin, ed., (Fermilab, 1989) 133; T. Ypsilantis and J. Seguinot, Nucl. Instrum. and Meth. **343** (1994) 30.
- [6] D. Leith, Nucl. Instrum. and Meth. **A265** (1988) 120.
- [7] K. Ashktorab, et al., BRAHMS Conceptual Design Report, Brookhaven National Laboratory (October 1994).

- [8] See, e.g., *Proc. of the Seminar held on the Occasion of the 50th Anniversary of the Discovery of Vavilov-Čerenkov Radiation*, P. Carlson, ed., Nucl. Instrum. and Meth. **A248** (1986).
- [9] T. Sugitate, et al., Nucl. Instrum. and Meth. **A307**, (1991) 265.
- [10] R. Debbe, et al., “RD-44: Development of a RICH Detector for BRAHMS”, Internal BRAHMS Note #5 (1994).
- [11] Hamamatsu Corp., Bridgewater, NJ 08807.
- [12] Edmund Scientific Co., Barrington, NJ 08007.
- [13] S.W. Benson, *Thermochemical Kinetics*, (Wiley, New York, 1968) Chapt. 2.
- [14] R.C. Reid, J.M. Prausnitz and B.E. Poling, *The Properties of Gases and Liquids*, (McGraw-Hill, New York, 4th ed., 1987).
- [15] E.R. Hayes, R.A. Schluter and A. Tamosaitis, Argonne National Laboratory Report ANL-6916 (1964).
- [16] PCR Inc., Gainesville, FL 32602.

Figure Captions

Fig. 1. Single photoelectron ADC distributions from LED measurements a) for the Hamamatsu multi-anode PMT b) for an RCA 8854 PMT.

Fig. 2. Position dependence of the PMT pulse height in three adjacent pixels, measured as the position of an LED is stepped with respect to the phototube.

Fig. 3. Schematic view of the prototype RICH counter. See text for details.

Fig. 4. Schematic flow-diagram for gas-handling system. Solid lines are for initial filling with the fluorocarbon; dashed lines (note reversed direction) are for final recovery of the fluorocarbon gas. With this system, the pressure in the RICH vessel can be kept within $< 10\%$ of atmospheric over both the filling and recovery operations.

Fig. 5. Results from the prototype RICH counter with test beam at $12 \text{ GeV}/c$ and a Freon gas mixture. Panel a shows a ring image from approximately 1100 events and panels b and c show the ADC pulse height spectra from two individual pixels. See text for details.

Fig. 6. Results from the prototype RICH counter with test beam at $3 \text{ GeV}/c$ and a C_4F_{10} -Ar gas mixture. Panels a, b and c show individual events with fitted rings; the ring centers are shown as stars and come from independent drift chamber tracking; the box sizes are proportional to the pulse height in each pixel. Panel d is a histogram of the fitted ring radius from the entire run, showing peaks identified as π^- , μ^- and e^- .

Fig. 7. The mean radius from event-by-event fits to rings in the prototype RICH counter filled with a C_4F_{10} -Ar gas mixture, for different particle species. The solid curves show the expected radii for an index of refraction of $n = 1.00113$; the shaded regions represent a 5% systematic uncertainty in the absolute momentum scale.

	b.p. (°C)	M (g/mol)	C_p (Joule/mol·K)	v.p. (atm.)	$(n - 1) \times 10^6$
N ₂	-196	28.1	29.12	—	285
Ar	-186	39.9	20.79	—	269
Freon-12	-30	120.9	73.35	5.77	1180
C ₄ F ₁₀	-2	238.0	243.56	3.24	1415

Table 1

Properties of radiator gases used in the results of this paper. Listed are the boiling point (b.p.) in degrees Celsius, the molecular weight (M), the constant-pressure heat capacity (C_p) at 300 K, the vapor pressure (v.p.) in atmospheres, and $(n-1)\times 10^6$, where n is the index of refraction at 1 atm. pressure, 300 K and a wavelength of 300 nm ($E=4.1$ eV). The value of C_p for C₄F₁₀ was calculated using the method of Benson (Ref. [13]) and the tables in Ref. [14]. The index of refraction for Freon-12 is deduced from the data given in Ref. [15]. The index of refraction for C₄F₁₀ was calculated using the Lorentz-Lorenz Equation and measurements reported in Ref. [5].

This figure "fig1-1.png" is available in "png" format from:

<http://arxiv.org/ps/hep-ex/9503006v1>

This figure "fig1-2.png" is available in "png" format from:

<http://arxiv.org/ps/hep-ex/9503006v1>

This figure "fig1-3.png" is available in "png" format from:

<http://arxiv.org/ps/hep-ex/9503006v1>

This figure "fig1-4.png" is available in "png" format from:

<http://arxiv.org/ps/hep-ex/9503006v1>

This figure "fig1-5.png" is available in "png" format from:

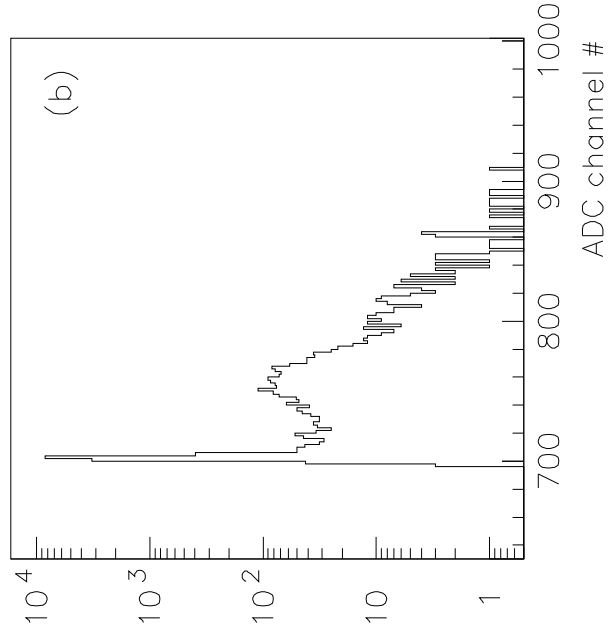
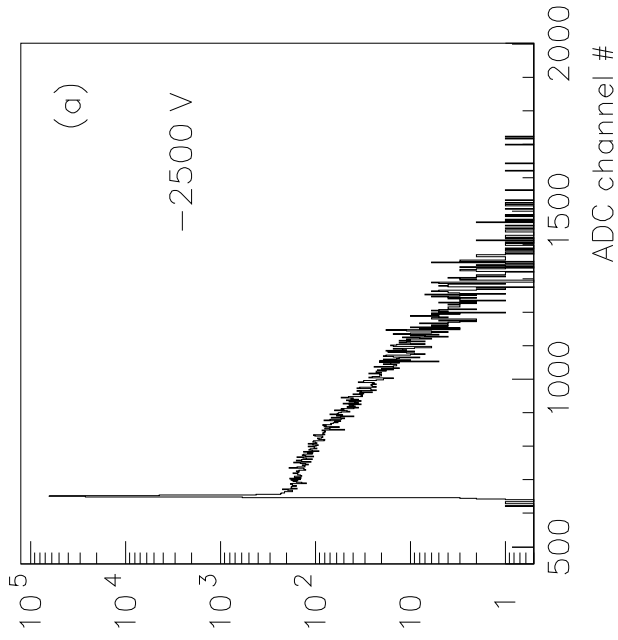
<http://arxiv.org/ps/hep-ex/9503006v1>

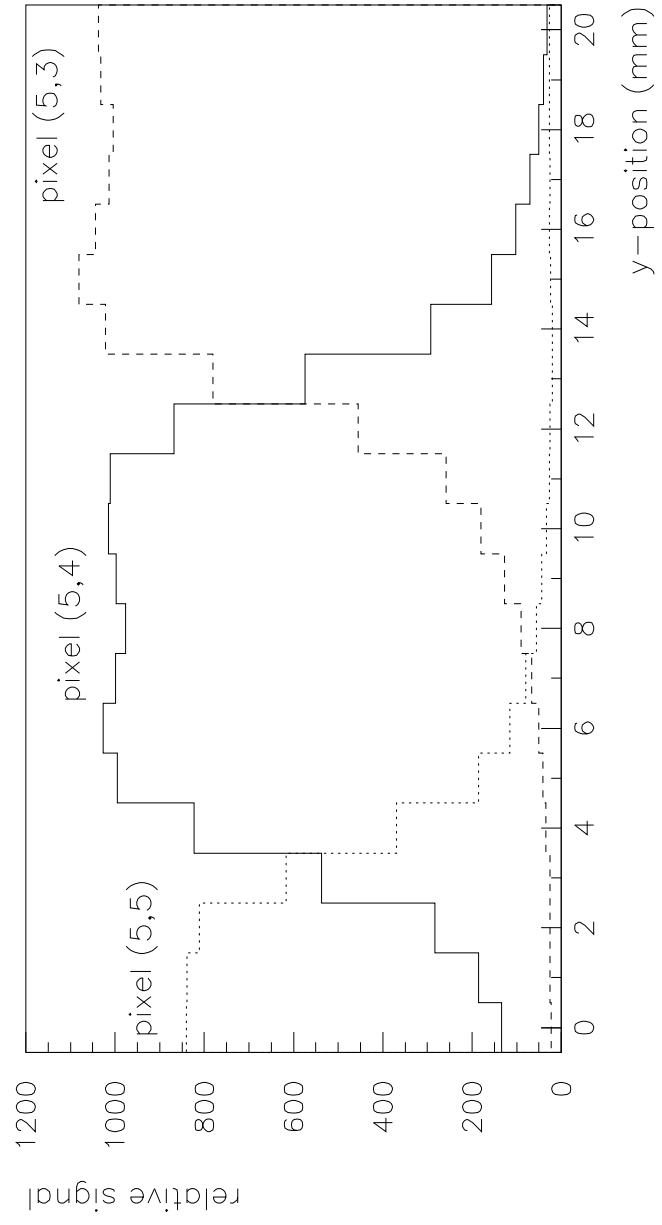
This figure "fig1-6.png" is available in "png" format from:

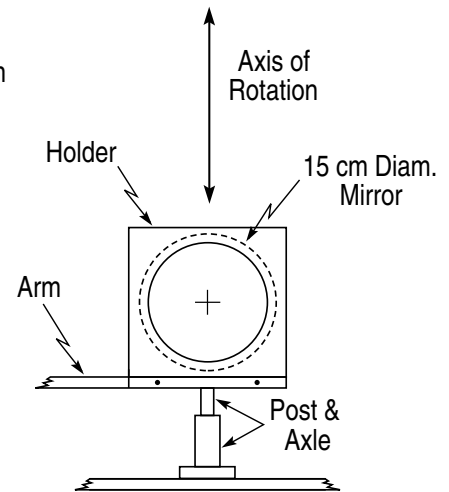
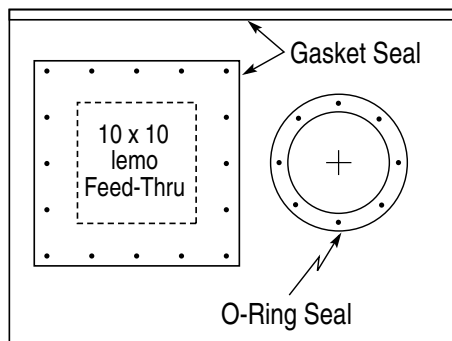
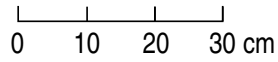
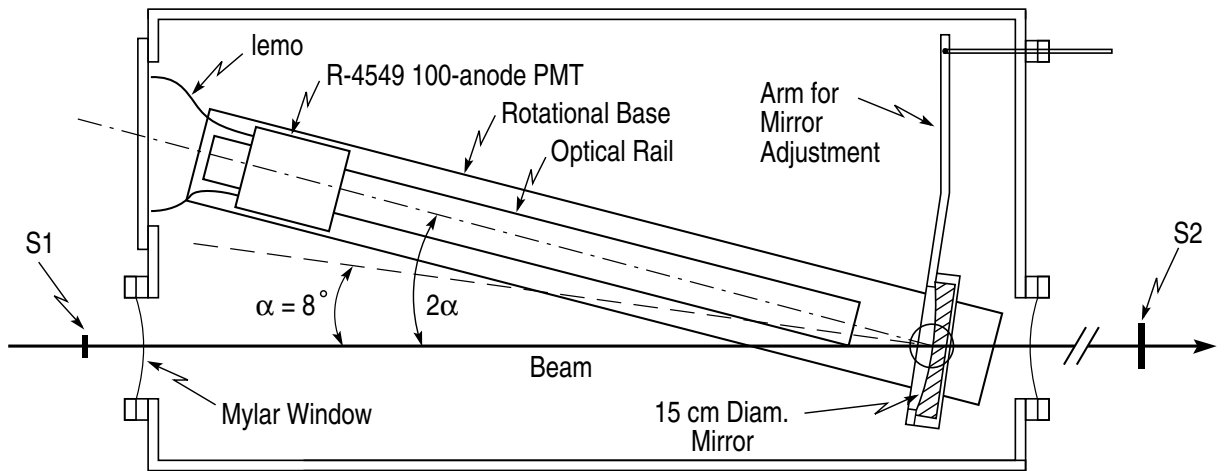
<http://arxiv.org/ps/hep-ex/9503006v1>

This figure "fig1-7.png" is available in "png" format from:

<http://arxiv.org/ps/hep-ex/9503006v1>







END VIEW (b)

MIRROR ASSEMBLY (c)

